RIS Optimization on the Complex Circle Manifold for Interference Mitigation in Interference Channels

Mohamed A. ElMossallamy, *Member, IEEE,* Karim G. Seddik, *Senior Member, IEEE,* Wei Chen, *Senior Member, IEEE,* Li Wang, *Senior Member, IEEE,* Geoffery Ye Li, *Fellow, IEEE* and Zhu Han, *Fellow, IEEE*

***Abstract*—In this paper, we investigate the use of reconfigurable intelligent surfaces (RIS) to allow multiple user pairs to communicate simultaneously over the same channel. We propose a Riemannian manifold optimization approach to solve the problem of configuring the RIS passive reflection coefficients to minimize the total interference under constant modulus constraints. We compare the proposed approach to the widely-used semidefinite relaxation approach (SDR) for dealing with the constant modulus constraints. We investigate, using extensive numerical simulations, the effects of various system parameters, such as the number of users, the number of RIS elements, and the fraction of power received through the RIS. Our results demonstrate that RISs can substantially minimize interference allowing multiple user pairs to simultaneously communicate over the same channel and that the proposed approach vastly outperforms the semidefinite relaxation-based approach, which fails to find satisfactory solutions.**

I. Introduction

Reconfigurable intelligent surfaces (RISs) are envisioned to be one of the main enabling technologies for beyond-5G wireless communication systems [1], [2]. An RIS is comprised of a large number of tightly-packed nearly-passive elements capable of interacting with incident electromagnetic waves in a controllable manner [3], [4]. By placing RISs in an environment where wireless communication is taking place, the propagation of the transmitted signals can be partially controlled by changing the interaction of RISs with the ambient electromagnetic waves giving rise to a smart radio environment [1], in which the effective channels perceived by the wireless transceivers can be controlled.

Motivated by the vast potential enabled by the ability to control the wireless channel, researchers have set to investigate the use of RISs in various communications scenarios ranging from traditional single-user and multi-user channels to unmanned aerial vehicles (UAV) enabled networks [5]. Early research results have demonstrated the utility of RISs in various communications scenarios. Single-user scenarios have been considered in [6]–[9]. In [6], beamforming at the base station and the passive reflection coefficients at the RIS has been optimized, either centrally using semidefinite relaxation or in a distributed manner utilizing alternating optimization. In [7], suboptimal algorithms based on alternating optimization and successive convex approximation have been proposed for RIS optimization in a wideband OFDM system. Moreover, data-driven deep-learning-based approaches has been proposed either based on partial channel information [8], or position data [9].

Multi-user scenarios have been considered in [10]–[14]. In [10], zero-forcing precoding is used at the base station to eliminate inter-user interference and simplify the RIS coefficient optimization problem, which is solved using sequential fractional programming to maximize the total energy efficiency. In [11], the schemes in [6] are extended to multiuser scenarios. In [12], suboptimal algorithms based on the alternating direction method of multipliers (ADMM) have been proposed to solve the problem of weighted sum-rate maximization in an RIS-assisted downlink. A hybrid beamforming framework has been proposed in [13] to jointly optimize the digital beamforming at the base station and analog beamforming at the RIS to maximize the achievable sum-rate. In [14], deep reinforcement learning (DLR) has been applied to solve the joint optimization of beamforming at the base station and the RIS, and found to be competitive with alternating optimization techniques.

The use of the RIS to manage interference when multiple use pairs are sharing the channel has been considered before in [15], [16]. In [15], it has been experimentally demonstrated that an RIS is capable of reducing the interference to a communicating pair from one transmitter by up to 30 dB, while in [16], a cognitive communication system was considered, and an RIS was exploited to maximize the rate achievable for the secondary user (SU) given a signal-to-interference-plus-noise ratio (SINR) constraint for the primary user (PU).

In this paper, we investigate a more general case of using reconfigurable intelligent surfaces to allow simultaneous communication among K different communicating pairs over an interference channel. We formulate an optimization problem to minimize the total interference between all communicating pairs. To deal with the non-convex constant modulus constraints on the RIS reflection coefficients, we propose a Riemannian manifold optimization approach that interprets these constraints geometrically as restricting the feasible set to be the surface of the complex circle manifold [17]. We use extensive numerical simulations to evaluate the performance of

Mohamed A. ElMossallamy and Zhu Han are with the Electrical and Computer Engineering Department, University of Houston, TX, USA. Zhu Han is also with the Department of Computer Science and Engineering, Kyung Hee University, Seoul, South Korea (emails: m.ali@ieee.org, zhan2@uh.edu).

Karim G. Seddik is with the Electronics and Communications Engineering Department, American University in Cairo, New Cairo, Egypt (email: kseddik@aucegypt.edu).

Wei Chen is with the Department of Electronic Engineering, Tsinghua University, Beijing, China (email: wchen@tsinghua.edu.cn).

Li Wang is with the School of Electronic Engineering, Beijing University of Posts and Telecommunications, Beijing, China (email: liwang@bupt.edu.cn).

Geoffrey Ye Li is with the Department of Electrical and Electronic Engineering, Imperial College London, London, UK (email: Geoffrey.Li@imperial.ac.uk).

the proposed manifold optimization method and investigate the effects of changing various parameters such as the number of users, the number of RIS elements, and the fraction of power received through the RIS. Our results show that the proposed approach can effectively minimize interference between the users allowing simultaneous communications in the same channel at rates close to what is achievable if the other users did not exist. In contrast, the baseline semidefinite relaxation approach fails to find adequate solutions for the formulated problem.

II. System Model

We consider a scenario where K single-antenna transmitters aim to communicate with corresponding K single-antenna receivers assisted by an RIS that partially controls the propagation between the nodes. The received signal at the k-th receiver can be written as

$$\begin{aligned} y_k = &\underbrace{d_{k,k}s_k + \left(\sum_{\ell=1}^{L} \psi_\ell f_{k,\ell} g_{\ell,k}\right) s_k}_{\text{desired}} \\ &+ \underbrace{\sum_{\mathsf{k}\neq k} d_{k,\mathsf{k}} s_{\mathsf{k}} + \sum_{\mathsf{k}\neq k} \left(\sum_{\ell=1}^{L} \psi_\ell f_{\mathsf{k},\ell} g_{\ell,\mathsf{k}}\right) s_{\mathsf{k}}}_{\text{interference}} + w_k, \end{aligned} \tag{1}$$

where w_k denotes the noise at the k-th receiver, $d_{k,\mathsf{k}}$ is the channel coefficient between the k-th transmitter and the k-th receiver, ψ_ℓ is the reflection coefficient applied at the ℓ-th element of the RIS, $f_{k,\ell}$ is the channel coefficient between the k-th transmitter and the ℓ-th element of the RIS, $g_{\ell,k}$ is the channel coefficient between the ℓ-th element of the RIS and the k-th receiver, and s_k is the symbol emitted by the k-th transmitter. Hence, the first two terms constitute the desired signal received via the direct channel and through the RIS, respectively, and the last two terms constitute undesired interference terms.

The signal model can be expressed in an equivalent matrix form as

$$\begin{aligned} \mathbf{y} &= (\mathbf{D} + \mathbf{FQG})\,\mathbf{s} + \mathbf{w}, \\ \mathbf{y} &= \mathbf{H}_{\text{eff}}\ \mathbf{s} + \mathbf{w}, \end{aligned} \tag{2}$$

where $\mathbf{y} = [y_1, y_2, \ldots, y_K]$, $\mathbf{s} = [s_1, s_2, \ldots, s_K]$, $\mathbf{D} \in \mathbb{C}^{K\times K}$ comprise the direct channel coefficients between the set of transmitters and the set of receiver, $\mathbf{F} \in \mathbb{C}^{K\times L}$ comprises the channel coefficients between the set of transmitters and the elements of the RIS, $\mathbf{G} \in \mathbb{C}^{L\times K}$ comprises the channel coefficients between the elements of the RIS and the set of receivers, $\mathbf{Q} = \operatorname{diag}(\psi_1, \psi_2, \ldots, \psi_L)$ denotes the RIS interaction matrix, and $\mathbf{H}_{\text{eff}} \triangleq \mathbf{D} + \mathbf{FQG}$. Note that although this model looks like a MIMO link, the sets of the transmitters/receivers cannot cooperate to transmit/decode their respective signals, which is a fundamental difference compared to MIMO links. Similar to [10], [11], [14], it is assumed that the RIS has knowledge of all the relevant channels which are assumed to be Rayleigh distributed[1].

[1]It is worth mentioning that obtaining channel knowledge at the RIS is a daunting task because of the passive nature of the RIS elements; however, some techniques have been proposed in the literature, e.g., [18].

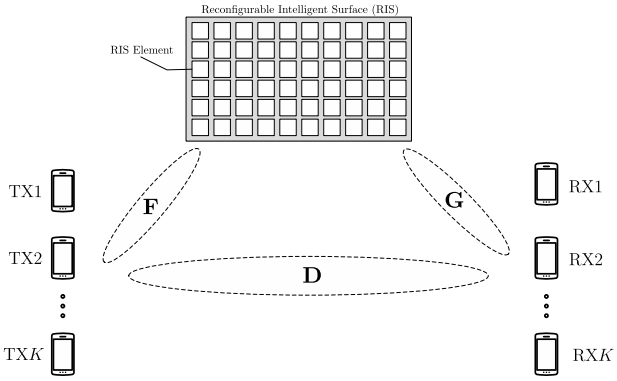

Fig. 1. The system model. K different user pairs simultaneously communicating assisted by an RIS to minimize interference.

The (i-th, j-th) element of the overall effective channel, $\mathbf{H}_{\text{eff}}$, between the set of transmitters and set of receivers can be expressed as

$$[\mathbf{H}_{\text{eff}}]_{i,j} = d_{i,j} + \sum_{\ell=1}^{L} \psi_\ell f_{i,\ell} g_{\ell,j}. \tag{3}$$

The diagonal terms of the effective channel matrix, i.e., $\left\{[\mathbf{H}_{\text{eff}}]_{i,j}\right\}_{i=j}$, constitute desired paths, and the off-diagonal terms, i.e., $\left\{[\mathbf{H}_{\text{eff}}]_{i,j}\right\}_{i\neq j}$, constitute undesired interfering paths. Our goal in this paper is to find configurations of the RIS elements that minimize the undesired interfering paths allowing simultaneous communications by all pairs at satisfactory rates.

III. Interference Minimization using RIS

In this section, we present a manifold optimization-based approach for RIS optimization for interference minimization. The commonly used semidefinite relaxation (SDR)-based approach serves as a benchmark to judge the performance of the proposed approach.

First, we reformulate the problem in the more familiar quadratic form, which is also needed for the SDR-based approach. We start by writing the vectorized form of the overall effective matrix as

$$\begin{aligned} \operatorname{vec}(\mathbf{H}_{\text{eff}}) &= \operatorname{vec}(\mathbf{D}) + \operatorname{vec}(\mathbf{FQG}), \\ &= \operatorname{vec}(\mathbf{D}) + \left(\mathbf{G}^{\mathsf{T}} \otimes \mathbf{F}\right) \operatorname{vec}(\mathbf{Q}), \end{aligned} \tag{4}$$

where $\operatorname{vec}(\cdot)$ denotes linear column-wise vectorization operator, $(\cdot)^{\mathsf{T}}$ denotes the matrix transpose, $\otimes$ denotes the Kronecker matrix product, and we have used the identity $\operatorname{vec}(\mathbf{ABC}) = \left(\mathbf{C}^{\mathsf{T}} \otimes \mathbf{A}\right) \operatorname{vec}(\mathbf{B})$.

Let $\mathbf{C} = \left(\mathbf{G}^{\mathsf{T}} \otimes \mathbf{F}\right)$, and note that $\operatorname{vec}(\mathbf{Q})$ has only L non-zero elements since $\mathbf{Q} = \operatorname{diag}(\psi_1, \psi_2, \ldots, \psi_L)$. Hence, we can rewrite (4) as

$$\operatorname{vec}(\mathbf{H}_{\text{eff}}) = \mathbf{d} + \mathbf{R}\boldsymbol{\psi}, \tag{5}$$

where $\mathbf{d} = \operatorname{vec}(\mathbf{D})$, the ℓ-th column of $\mathbf{R} \in \mathbb{C}^{K^2\times L}$ is given by the $(L(\ell-1)+\ell)$-th column of $\mathbf{C}$, and $\boldsymbol{\psi} = [\psi_1, \psi_2, \ldots, \psi_L]$.

We are only concerned with elements of (5) that correspond to the off-diagonal elements of $\mathbf{H}_{\text{eff}}$, i.e., elements corresponding to interfering paths, cf. (1) and (3). Define the set $\mathcal{I} = \left\{i : i \in 0, 1, \ldots, K^2-1, i \mod (K+1) \neq 0\right\}$. Let

vector $\mathbf{u}$ comprise the elements of $\mathbf{d}$ whose indices fall in $\mathcal{I}$. Similarly, let the matrix $\mathbf{Z} \in \mathcal{C}^{(K^2-K)\times L}$ comprise the rows of $\mathbf{R}$ whose indices fall in the set $\mathcal{I}$. Hence, we can write the problem of minimizing the interference as

$$\underset{\boldsymbol{\psi}}{\text{minimize}} \quad \|\mathbf{u} + \mathbf{Z}\boldsymbol{\psi}\|^2 \tag{6a}$$

$$\text{subject to} \quad |\psi_i| = 1 \ \forall i = 1, 2, \ldots, L. \tag{6b}$$

This problem is non-convex because of the constant modulus constraints and is NP-hard in general. There is no general approach to solve (6) optimally in polynomial time. Nevertheless, we present two techniques to find a sub-optimal solution efficiently.

A. Semidefinite Relaxation-based Benchmark

The non-convexity of the problem in (6) arises from the constant modulus constraint on the RIS reflection coefficients. The most commonly used technique in the literature to deal with this problem is to relax it into a convex Semidefinite program (SDP). First, we reformulate (6) to an equivalent, still non-convex, quadratically-constrained quadratic program (QCQP) given by

$$\underset{\boldsymbol{\psi}}{\text{minimize}} \quad \mathbf{u}^{\mathsf{H}}\mathbf{u} + 2\mathbf{u}^{\mathsf{H}}\mathbf{Z}\boldsymbol{\psi} + \boldsymbol{\psi}^{\mathsf{H}}\mathbf{Z}^{\mathsf{H}}\mathbf{Z}\boldsymbol{\psi} \tag{7a}$$

$$\text{subject to} \quad |\psi_i|^2 = 1 \ \forall i = 1, 2, \ldots, L, \tag{7b}$$

where $(\cdot)^{\mathsf{H}}$ denotes the Hermitian transpose of a matrix. The quadratic form in the objective function (7a) can be made homogeneous by introducing an auxiliary variable. In particular, we can write an equivalent problem as

$$\underset{\mathbf{v}}{\text{minimize}} \quad \mathbf{v}^{\mathsf{H}}\ \mathbf{C}\ \mathbf{v} \tag{8a}$$

$$\text{subject to} \quad |v_i| = 1 \ \forall i = 1, 2, \ldots, L, \tag{8b}$$

where

$$\mathbf{C} = \begin{bmatrix} \mathbf{Z}^{\mathsf{H}}\mathbf{Z} & \mathbf{Z}^{\mathsf{H}}\mathbf{u} \\ \mathbf{u}^{\mathsf{H}}\mathbf{Z} & \mathbf{u}^{\mathsf{H}}\mathbf{u} \end{bmatrix}, \qquad \mathbf{v} = \begin{bmatrix} \boldsymbol{\psi} \\ 1 \end{bmatrix}. \tag{9}$$

Let $\mathsf{tr}(\cdot)$ denote the matrix trace operator, and define $\mathbf{V} = \mathbf{v}\mathbf{v}^{\mathsf{H}}$. Thus, by making use of the fact that $\mathbf{v}^{\mathsf{H}}\mathbf{C}\mathbf{v} = \mathsf{tr}\big(\mathbf{v}^{\mathsf{H}}\mathbf{C}\mathbf{v}\big) = \mathsf{tr}\big(\mathbf{C}\mathbf{v}\mathbf{v}^{\mathsf{H}}\big)$, we can recast (9) as the semidefinite program given by

$$\underset{\mathbf{V}}{\text{minimize}} \quad \mathsf{tr}(\mathbf{C}\mathbf{V}) \tag{10a}$$

$$\text{subject to} \quad \mathbf{V}_{\ell,\ell} = 1 \ \forall \ell = 1, 2, \ldots, L+1, \tag{10b}$$

$$\mathbf{V} \succeq 0, \tag{10c}$$

where the rank-one constraint on $\mathbf{V}$ has been relaxed to make the problem convex. This SDP can be solved using any standard semidefinite solver, e.g., SeDuMi [19]. If the solver gets a rank-one solution $\mathbf{V}$, the optimal $\mathbf{v}$ and subsequently $\boldsymbol{\psi}$, can be directly extracted from it; otherwise, an approximate sub-optimal rank-one solution can be extracted using various techniques [6]. Note that the matrix $\mathbf{C}$ is highly rank deficient, which has ramifications on the performance of the SDP approach discussed later in Sec. V.

B. Proposed Manifold Optimization-based Technique

The unit modulus constraints on the RIS reflection coefficients can be geometrically interpreted as restricting the solution to lie on the surface of a smooth Riemannian manifold embedded in $\mathbb{C}^L$. In particular, each optimization variable, ψ_ℓ lives on a continuous search space given by the complex circle denoted by

$$\mathcal{S} = \{x \in \mathbb{C} : x^* x = 1\}. \tag{11}$$

The complex circle, $\mathcal{S}$, is a smooth Riemannian sub-manifold of $\mathbb{C}$. The feasible set of the L RIS reflection coefficients is the Cartesian product of L complex circles, i.e.,

$$\underbrace{\mathcal{S} \times \mathcal{S} \times \cdots \times \mathcal{S}}_{L \text{ times}}. \tag{12}$$

This product of smooth Riemannian manifolds is itself a smooth Riemannian sub-manifold of $\mathbb{C}^L$ known as the complex circle manifold and formally defined as

$$\mathcal{S}^L = \left\{\mathbf{x} \in \mathbb{C}^L : |x_1| = |x_2| = \cdots = |x_L| = 1\right\}. \tag{13}$$

Hence, if no other constraints exist, the problem of optimizing the RIS reflection coefficients can be formulated as an unconstrained problem on the surface of complex circle manifold, $\mathcal{S}^L$, whereby gradient-based unconstrained *manifold optimization algorithms* can be then be used to find a solution efficiently. Encouraging results using this technique have been reported in hybrid beamforming, e.g., [20], and single-user RIS-assisted MISO links optimization [21].

An unconstrained manifold optimization problem [17] takes the following form

$$\underset{\boldsymbol{\psi} \in \mathcal{M}}{\text{minimize}} \quad f(\boldsymbol{\psi}), \tag{14}$$

where $\mathcal{M}$ is a Riemannian manifold and $f : \mathcal{M} \to \mathbb{R}$ is some smooth real-valued objective function to be optimized. Hence, the problem in (6) can be cast in the form of (14), where $\mathcal{M}$ is $\mathcal{S}^L$ and $f(\boldsymbol{\psi}) = \|\mathbf{u} + \mathbf{Z}\boldsymbol{\psi}\|^2$.

Similar to Euclidean spaces, a gradient-descent algorithm on Riemannian manifolds consists of two main steps. First, a descent direction must be found; second, the length of the step along the descent direction must be chosen. The solution is updated iteratively by repeating these steps until convergence. However, these steps are adapted to address the geometric nature of the manifold and are explained next.

The tangent space at a point, $\mathbf{x}_m$, on the complex circle manifold, $\mathbf{x}_k$, $T_{\mathbf{x}_m}\mathcal{M}$, is defined as the space of tangent vectors of all smooth curves passing through $\mathbf{x}_m$ and is given by

$$T_{\mathbf{x}_m}\mathcal{M} = \left\{\mathbf{v} \in \mathbb{C}^L : \Re\left(\mathbf{v} \odot \mathbf{x}_m^* = \mathbf{0}_L\right)\right\}, \tag{15}$$

where $\Re\{\cdot\}$ and $\odot$ denote the element-wise real-part of a complex vector and the Hadamard element-wise multiplication, respectively. The direction of the greatest increase of the objective function at a given point on the manifold, $\mathbf{x}_m$, but restricted to its tangent space, is called the "Riemannian gradient", which is computed numerically by computing the Euclidean gradient at this point then projecting it onto the tangent space via a projection operator.

The projection operator from the ambient Euclidean space onto the tangent space at a point $\mathbf{x}_m$ on the complex circle manifold, i.e., $T_{\mathbf{x}_m}\mathcal{M}$, is given by [17]

$$\mathcal{P}_{T_{\mathbf{x}_m}\mathcal{M}}(\mathbf{v}) = \mathbf{v} - \Re\{\mathbf{v} \odot \mathbf{x}_m^*\} \odot \mathbf{x}_m. \tag{16}$$

Hence, the Riemannian gradient of an objective function f on the complex circle manifold can be expressed as

$$\begin{aligned}\nabla_{\mathcal{M}} f(\mathbf{x}_m) &= \mathcal{P}_{T_{\mathbf{x}_m}\mathcal{M}}(\nabla f(\mathbf{x}_m)) \\ &= \nabla f(\mathbf{x}_m) - \Re\{\nabla f(\mathbf{x}_m) \odot \mathbf{x}_m^*\} \odot \mathbf{x}_m.\end{aligned} \tag{17}$$

For our problem, the Euclidean gradient, $\nabla f(\mathbf{x}_m)$, is given by

$$\nabla f(\mathbf{x}_m) = 2\mathbf{Z}^{\mathsf{H}}(\mathbf{u} + \mathbf{Z}\mathbf{x}_m). \tag{18}$$

At a given point, $\mathbf{x}_m$, on the manifold, a descent direction $\boldsymbol{\eta}_m$ in the tangent space $T_{\mathbf{x}_m}\mathcal{M}$ can be found based on the *Riemannian gradient* such that $\langle \boldsymbol{\eta}_m, \nabla f(\mathbf{x}_m)\rangle < 0$. However, the solution cannot be simply updated via $\hat{\mathbf{x}}_{m+1} = \mathbf{x}_m + \alpha_m \boldsymbol{\eta}_m$, since $\hat{\mathbf{x}}_{m+1}$ would lie in the tangent space $T_{\mathbf{x}_m}\mathcal{M}$ and not on the surface of the manifold. Hence, an additional mapping is needed from the tangent space to the surface of the manifold. This mapping is referred to as a *retraction*, which for the case of the complex circle manifold can be defined as [17]

$$\mathcal{R}(\mathbf{v}) = \mathbf{v} \oslash |\mathbf{v}|, \tag{19}$$

where $|\cdot|$ and $\oslash$ denote element-wise absolute value and element-wise Hadamard division, respectively.

Equipped with the Riemannian gradient obtained via a projection mapping and the retraction mapping, a steepest-descent procedure can be used to find a locally optimal solution for (14). However, the steepest descent algorithm is known to be slow in practice. Hence, we use the Polak-Ribiére conjugate gradient algorithm, which incorporates second-order information and is known to converge superlinearly. The manifold generalization of the Polak-Ribiére descent direction at the $(m+1)$-th iteration is given by

$$\boldsymbol{\eta}_{m+1}^{\mathcal{M}} = -\nabla_{\mathcal{M}} f(\mathbf{x}_{m+1}) + \beta_{m+1}^{\mathrm{PR}-\mathcal{M}} \mathcal{T}_{\mathbf{x}_m \mapsto \mathbf{x}_{m+1}}(\boldsymbol{\eta}_m), \tag{20}$$

where $\beta_{m+1}^{\mathrm{PR}-\mathcal{M}}$ is the manifold generalization of the Polak-Ribiére's conjugate parameter and $\mathcal{T}_{\mathbf{x}_m \mapsto \mathbf{x}_{m+1}} : T_{\mathbf{x}_m}\mathcal{M} \mapsto T_{\mathbf{x}_{m+1}}\mathcal{M}$ is a vector transport operation needed to add/subtract points on different tangent spaces. In the case of the complex circle manifold, the vector transport operation can be expressed as

$$\mathcal{T}_{\mathbf{x}_m \mapsto \mathbf{x}_{m+1}}(\mathbf{v}) = \mathbf{v} - \Re\{\mathbf{v} \odot \mathbf{x}_{m+1}^*\} \odot \mathbf{x}_{m+1}, \tag{21}$$

which is equivalent to an additional projection from the old tangent space to the new tangent space, cf. (16), while the Polak-Ribiére's conjugate parameter is given by

$$\beta_{m+1}^{\mathrm{PR}-\mathcal{M}} = \nabla f(\mathbf{x}_{m+1})^{\mathsf{H}} \frac{\left(\nabla f(\mathbf{x}_{m+1}) - \mathcal{T}_{\mathbf{x}_m \mapsto \mathbf{x}_{m+1}}(\nabla f(\mathbf{x}_m))\right)}{\|\nabla f(\mathbf{x}_m)\|^2}. \tag{22}$$

Finally, we have everything we need to iteratively update the solution using

$$\mathbf{x}_{m+1} = \mathcal{R}\left(\mathbf{x}_m + \tau_m \boldsymbol{\eta}_{m+1}^{\mathcal{M}}\right), \tag{23}$$

where τ_m is the step size at the m-th iteration. The well-known Armijo backtracking line search algorithm [17] can be used to choose the step size, which ensures that the objective function is non-increasing, i.e., $f(\mathbf{x}_{m+1}) \leq f(\mathbf{x}_m)$ at each iteration. The complete procedure is summarized in Algorithm 1.

Complexity Analysis: Before we conclude this section, we briefly summarize the computational complexity of each iteration of the proposed manifold optimization method. The computation of Euclidean gradient, cf. (18), takes $4L\left(K^2-K\right)$ flops. The projection to obtain the Riemannian gradient, cf. (17), takes $3L$ flops. Computing the Polak-Ribiére parameter, cf. (22), takes $6L$ flops, and the descent direction, cf. (**??**), takes an additional $5L$ flops. Finally, updating the solution via (23) takes $3L$ flops for a total of $17L + 4L\left(K^2-K\right)$. Note that it is reasonable to assume that the number of RIS elements is much larger than the number of users' pairs, i.e., $L \gg K$.

Algorithm 1: Manifold-based RIS Optimization for Interference Minimization

Initialize iteration number $m = 0$;
Initialize $\mathbf{x}_0$ to any point on the manifold $\mathcal{S}^L$;
while $|\nabla_{\mathcal{M}} f(\mathbf{x}_m)| < \epsilon$ **do**
  Compute the Euclidean gradient $\nabla f(\mathbf{x}_m)$ using (18);
  Compute the Riemannian gradient $\nabla_{\mathcal{M}} f(\mathbf{x}_m)$ using (17);
  Compute the Polak-Ribiére parameter $\beta_{m+1}^{\mathrm{PR}-\mathcal{M}}$ using (22);
  Compute the descent direction $\boldsymbol{\eta}_{m+1}$ using (20);
  Calculate updated solution, $\mathbf{x}_{m+1}$ according to (23);
  $m = m + 1$;
Return $\boldsymbol{\psi} = \mathbf{x}_m$

IV. Numerical Results

In this section, we evaluate the proposed manifold optimization for interference minimization and compare it to the widely-used semidefinite relaxation as a benchmark. The performance is evaluated based on the achievable rate per user, which can be computed as

$$R_k = \log_2(1 + \gamma_k), \tag{24}$$

where γ_k denote the SINR for the k-th receiver which can be computed from

$$\gamma_k = \frac{\left|[\mathbf{H}_{\mathrm{eff}}]_{k,k}\right|^2}{\sum\limits_{j \neq k}\left|[\mathbf{H}_{\mathrm{eff}}]_{k,j}\right|^2 + \sigma_{n,k}^2}, \tag{25}$$

where $[\mathbf{H}_{\mathrm{eff}}]_{k,k}$ is as defined in (3) and $\sigma_{n,k}^2$ is the noise variance at the k-th receiver. All channels' gains are assumed to follow the Rayleigh distribution, and in lieu of using path loss models, we normalize the channels such that a single parameter, α, denotes the fraction of power received through the RIS.

Fig. 2 shows the achievable rate per user for different numbers of users' pairs, K, averaged over 10^3 channel realizations. The number of RIS elements $L = 100$, and the power fraction $\alpha = 0.5$. From the figure, the proposed MO-based approach effectively minimizes interference allowing simultaneous communications at rates approaching the case when no interference exists, i.e., off-diagonal elements are zeroed, for up to 6 user pairs. However, as the number of user pairs increases to 8, the performance deteriorates significantly. Note that although going from 6 to 8 user pairs is just a one-third increase, it almost doubles the number of interfering paths, $\left(K^2-K\right)$,

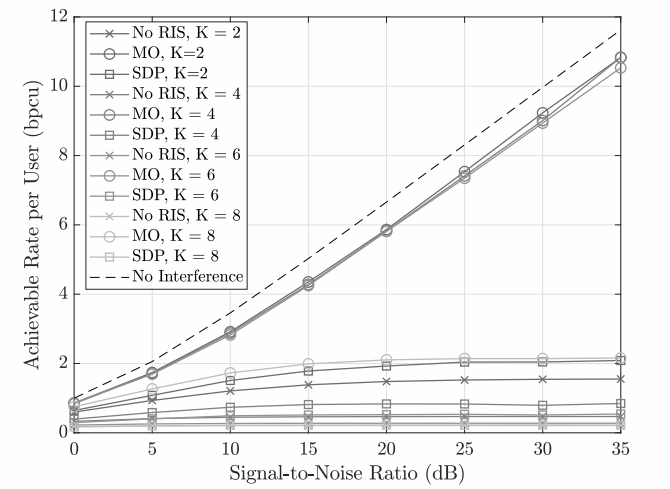

Fig. 2. The effects of the number user pairs, K, on the achievable rate when the reflection coefficients are optimized using the proposed manifold optimization (MO) approach. $L = 100$, $\alpha = 0.5$ for all curves. The achievable rate when the reflection coefficients are optimized using SDR is also shown as a benchmark along with the no RIS and no interference cases.

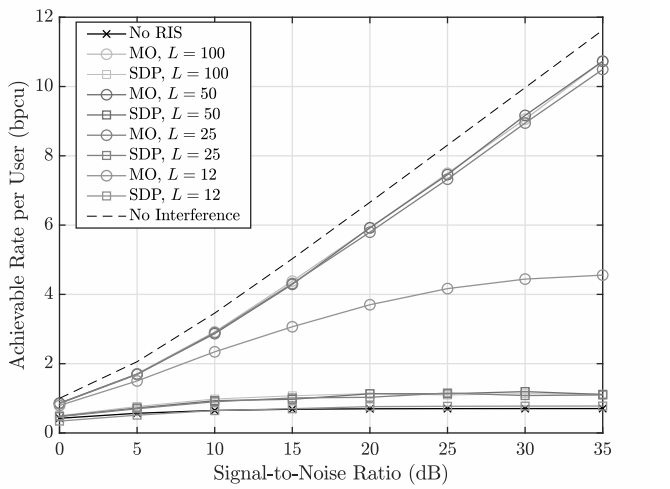

Fig. 3. The effects of the number of RIS elements, L, on the achievable rate when the reflection coefficients are optimized using the proposed manifold optimization (MO) approach. $K = 3, \alpha = 0.5$ for all curves. The achievable rate when the reflection coefficients are optimized using SDR is also shown as a benchmark along with the no RIS and no interference cases.

from 30 to 56. Meanwhile, the SDR approach fails to obtain a satisfactory solution for any of the considered cases. Note that all users enjoy the same performance since the channel model is symmetric, and the optimization algorithms minimize all interference equally.

Remark. It is worth discussing why the SDR approach fails in the considered problem, while it performs satisfactorily in other scenarios, e.g., [6]. As we alluded in Sec. III, the coefficient matrix $\mathbf{C}$ in (10) is highly rank deficient; hence, the minimizer of $\mathtt{tr}(\mathbf{CV})$ obtained by the SDP solver will lie in the null space of $\mathbf{C}$. However, this null space is of dimensions $L + 1 - K \gg 1$ and so is the rank of the obtained solution $V^\star$; hence, any technique to obtain a rank-one approximation will be highly suboptimal. In [6], the formulated problem also had a highly rank-deficient coefficient matrix; however, it was a maximization problem, and the solution generally lies in the column space of the coefficient matrix, which is of limited dimensionality. Hence, a rank-one solution is more readily obtained without significant loss of optimality.

Fig. 3 shows the achievable rate per user for different numbers of RIS elements, L, averaged over 10^3 channel realizations. The number of user pairs is $K = 3$, and the power fraction is $\alpha = 0.5$. From the figure, the proposed MO-based approach effectively eliminates the majority of interference allowing simultaneous communications at rates approaching the no interference case with as little as 25 RIS elements, while the performance starts to deteriorate for $L = 12$. This is intuitively expected as the number of degrees of freedom afforded by the RIS needs to be large enough *relative to the number of interfering paths between users* to effectively suppress inter-user interference. However, it is still significantly better than the no-RIS case.

Finally, in Fig. 4, we show the achievable rate per user for different values of the power fraction parameter α averaged over 10^3 channel realizations. From the figure, for values of α as low as 0.125, i.e., -9 dB, the proposed MO-based approach effectively eliminates the majority of interference allowing

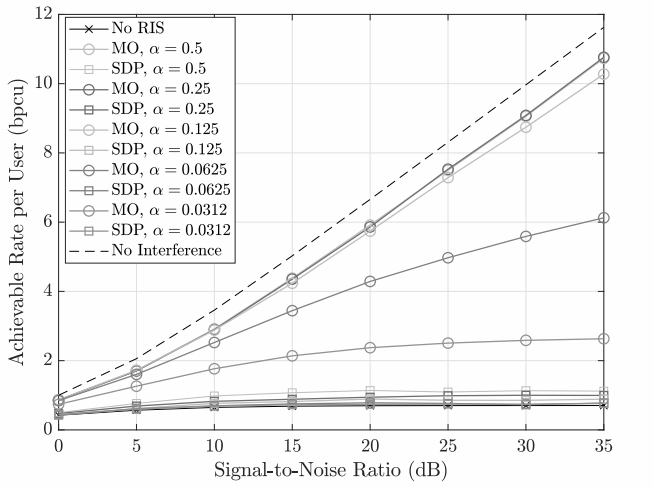

Fig. 4. The effects of the power fraction, α, on the achievable rate when the reflection coefficients are optimized using the proposed manifold optimization (MO) approach. $L = 100, K = 0.5$ for all curves. The achievable rate when the reflection coefficients are optimized using SDR is also shown as a benchmark along with the no RIS and no interference cases.

simultaneous communications at rates approaching the no interference case. However, as α decreases further, we start to see the RIS unable to remove all the interference. Nevertheless, it still allows communications at rates significantly better than the no-RIS case for α as low as 0.0312, i.e., -15 dB. Note that the performance can be improved for smaller α by increasing the number of RIS elements L.

V. Conclusion

In this paper, we have investigated the potential of using RISs to allow multiple user pairs to communicate simultaneously on the same channel. An interference minimization problem has been formulated to configure the RIS reflection coefficients. The constant-modulus constraints on the reflection coefficients of the RIS have been interpreted geometrically as restricting the feasible set to the surface of the complex

circle manifold, for which a Riemannian manifold optimization approach has been used to solve the formulated problem. Simulation results have shown that the proposed approach can be used to effectively minimize interference and allow simultaneous communication by multiple user pairs over the same channel at rates close to what they would have gotten if they had used the channel alone, while the widely-used SDR-based approach failed to find satisfactory solutions for the considered problem.

REFERENCES

[1] M. D. Renzo, M. Debbah, D.-T. Phan-Huy, A. Zappone, M.-S. Alouini, C. Yuen, V. Sciancalepore, G. C. Alexandropoulos, J. Hoydis, H. Gacanin, J. d. Rosny, A. Bounceur, G. Lerosey, and M. Fink, "Smart radio environments empowered by reconfigurable AI meta-surfaces: an idea whose time has come," *EURASIP J. Wireless Commun. and Netw.*, vol. 2019, no. 1, May 2019.

[2] C. Huang, S. Hu, G. C. Alexandropoulos, A. Zappone, C. Yuen, R. Zhang, M. D. Renzo, and M. Debbah, "Holographic MIMO surfaces for 6G wireless networks: Opportunities, challenges, and trends," *IEEE Wireless Commun.*, vol. 27, no. 5, pp. 118–125, Oct. 2020.

[3] E. Basar, M. Di Renzo, J. De Rosny, M. Debbah, M.-S. Alouini, and R. Zhang, "Wireless communications through reconfigurable intelligent surfaces," *IEEE Access*, vol. 7, pp. 116 753–116 773, 2019.

[4] M. A. ElMossallamy, H. Zhang, L. Song, K. G. Seddik, Z. Han, and G. Y. Li, "Reconfigurable intelligent surfaces for wireless communications: Principles, challenges, and opportunities," *IEEE Trans. on Cognitive Commun. and Netw.*, vol. 6, no. 3, pp. 990–1002, Sep. 2020.

[5] H. Hashida, Y. Kawamoto, and N. Kato, "Intelligent reflecting surface placement optimization in air-ground communication networks toward 6G," *IEEE Wireless Commun.*, vol. 27, no. 6, pp. 146–151, Dec. 2020.

[6] Q. Wu and R. Zhang, "Intelligent reflecting surface enhanced wireless network: Joint active and passive beamforming design," in *IEEE Global Commun. Conf. (GLOBECOM)*, Abu Dhabi, UAE, Dec. 2018.

[7] Y. Yang, S. Zhang, and R. Zhang, "IRS-enhanced OFDM: Power allocation and passive array optimization," in *IEEE Global Commun. Conf. (GLOBECOM)*, Waikoloa, HI, Dec. 2019.

[8] A. Taha, M. Alrabeiah, and A. Alkhateeb, "Deep learning for large intelligent surfaces in millimeter wave and massive MIMO systems," in *IEEE Global Commun. Conf. (GLOBECOM)*, Waikoloa, HI, Dec. 2019.

[9] C. Huang, G. C. Alexandropoulos, C. Yuen, and M. Debbah, "Indoor signal focusing with deep learning designed reconfigurable intelligent surfaces," in *IEEE Int. Workshop on Signal Process. Adv. in Wireless Commun. (SPAWC)*, Cannes, France, Jul. 2019.

[10] C. Huang, A. Zappone, G. C. Alexandropoulos, M. Debbah, and C. Yuen, "Reconfigurable intelligent surfaces for energy efficiency in wireless communication," *IEEE Trans. Wireless Commun.*, vol. 18, no. 8, pp. 4157–4170, Aug. 2019.

[11] Q. Wu and R. Zhang, "Intelligent reflecting surface enhanced wireless network via joint active and passive beamforming," *IEEE Trans. Wireless Commun.*, vol. 18, no. 11, pp. 5394–5409, Nov. 2019.

[12] H. Guo, Y.-C. Liang, J. Chen, and E. G. Larsson, "Weighted sum-rate maximization for intelligent reflecting surface enhanced wireless networks," in *IEEE Global Commun. Conf. (GLOBECOM)*, Waikoloa, HI, Dec. 2019.

[13] B. Di, H. Zhang, L. Li, L. Song, Y. Li, and Z. Han, "Practical hybrid beamforming with finite-resolution phase shifters for reconfigurable intelligent surface based multi-user communications," *IEEE Trans. Veh. Technol.*, vol. 69, no. 4, pp. 4565–4570, Apr. 2020.

[14] C. Huang, R. Mo, and C. Yuen, "Reconfigurable intelligent surface assisted multiuser MISO systems exploiting deep reinforcement learning," *IEEE J. Sel. Areas Commun.*, vol. 38, no. 8, pp. 1839–1850, Aug. 2020.

[15] X. Tan, Z. Sun, J. M. Jornet, and D. Pados, "Increasing indoor spectrum sharing capacity using smart reflect-array," in *IEEE Int. Conf. on Commun. (ICC)*, Kuala Lumpur, Malaysia, May 2016.

[16] X. Guan, Q. Wu, and R. Zhang, "Joint power control and passive beamforming in IRS-assisted spectrum sharing," *IEEE Communications Letters*, vol. 24, no. 7, pp. 1553–1557, Jul. 2020.

[17] P.-A. Absil, R. Mahony, and R. Sepulchre, *Optimization algorithms on matrix manifolds*. Princeton, N.J. ; Woodstock: Princeton University Press, 2008.

[18] Z. He and X. Yuan, "Cascaded channel estimation for large intelligent metasurface assisted massive MIMO," *IEEE Wireless Commun. Lett.*, vol. 9, no. 2, pp. 210–214, Feb. 2020.

[19] J. F. Sturm, "Using sedumi 1.02, a matlab toolbox for optimization over symmetric cones," *Optimization methods and software*, vol. 11, no. 1-4, pp. 625–653, 1999.

[20] X. Yu, J. Shen, J. Zhang, and K. B. Letaief, "Alternating minimization algorithms for hybrid precoding in millimeter wave MIMO systems," *IEEE J. Sel. Areas Commun.*, vol. 10, no. 3, pp. 485–500, Apr. 2016.

[21] X. Yu, D. Xu, and R. Schober, "MISO wireless communication systems via intelligent reflecting surfaces," in *IEEE/CIC Int. Conf. on Commun. in China (ICCC)*, Changchun, China, Aug. 2019, pp. 735–740.